

A cyanobacterial chemotaxis-like system controls phototactic orientation via phosphorylation of two antagonistic response regulators

Yu Han^{1,†}, Jonas Hammerl^{1,2,†}, Felicitas E. Flemming¹, Nils Schuergers^{1*}, Annegret Wilde^{1*}

¹Molecular Genetics, Institute of Biology III, Schänzlestraße 1, University of Freiburg, 79104 Freiburg, Germany

²Spemann Graduate School of Biology and Medicine (SGBM), Albertstr. 19A, University of Freiburg, Germany

*Corresponding authors. Molecular Genetics, Institute of Biology III, Schänzlestraße 1, University of Freiburg, 79104 Freiburg, Germany. E-mails: annegret.wilde@biologie.uni-freiburg.de, nils.schuergers@biologie.uni-freiburg.de

[†]These authors contributed equally to this work

Editor: [Carmen Buchrieser]

Abstract

Photosynthetic cyanobacteria exhibit phototaxis, utilizing type IV pili (T4P) to navigate either toward or away from a light source. The Tax1 system is a chemotaxis-like signal transduction pathway that controls the switch in cell polarity, which is crucial for positive phototaxis in *Synechocystis* sp. PCC 6803. The system consists of the blue/green light sensor PixJ, which controls the histidine kinase PixL and two CheY-like response regulators, PixG and PixH. However, the molecular mechanism by which Tax1 regulates T4P activity and polarity is poorly understood. Here, we investigated the phosphotransfer between PixL and its cognate response regulators *in vitro* and analyzed the localization and function of wild-type and phosphorylation-deficient PixG and PixH during phototaxis. We found that both PixG and PixH are phosphorylated by PixL but have different roles in phototaxis regulation. Only phosphorylated PixG interacts with the T4P motor protein PilB1 and localizes to the leading cell pole under directional light, thereby promoting positive phototaxis. In contrast, PixH is a negative regulator of PixG phosphorylation and inhibits positive phototaxis. We also demonstrated that the C-terminal receiver domain of PixL is essential for positive phototaxis, and modulates the kinase activity of PixL. Our findings reveal the molecular basis of positive phototaxis regulation by the Tax1 system and provide insights into the division of labor between PatA-type and CheY-like response regulators in cyanobacterial chemotaxis-like systems. Furthermore, these findings highlight similarities in the regulation of movement direction during twitching motility in phototactic and chemotactic bacteria.

Keywords: phototaxis; histidine kinase; response regulator; phosphorylation; CheY; PATAN

Introduction

Many bacteria control their movements in response to environmental stimuli. Photosynthetic cyanobacteria respond to light by migrating toward their preferred light conditions or evading potentially harmful illumination, a behavior termed positive or negative phototaxis. In cyanobacteria, including the unicellular model organism *Synechocystis* sp. PCC 6803 (hereafter *Synechocystis*), phototaxis requires type IV pili (T4P) (Bhaya et al. 2000, Yoshihara et al. 2001, Schuergers and Wilde 2015). T4P-dependent motility over wet surfaces relies on the extension, tethering, and retraction of pilus fibers, working like grappling hooks to pull the bacterial cell forward (Merz et al. 2000). This so-called twitching motility is powered by the secretion ATPases PilB and PilT, which dynamically interact with the inner membrane platform protein PilC to form motor complexes for the extension and retraction of T4P filaments, respectively (Jakovljevic et al. 2008, Takhar et al. 2013, Bischof et al. 2016). *Synechocystis* is capable of directional phototactic movement because single cells act as spherical micro-lenses, allowing them to detect the location of the light source (Schuergers et al. 2016). Focused light on the rear side of the cell, away from the light source, is suggested to lead to local excitation of photoreceptors or other signaling pathways. This cue activates

a signal transduction cascade that is thought to stimulate the polar localization of the extension ATPase PilB1, thereby promoting asymmetric T4P activity (Schuergers et al. 2015, 2016, Nakane and Nishizaka 2017, Nakane et al. 2022).

Cyanobacteria employ multiple receptors to perceive the spectral composition of light (Wiltbank and Kehoe 2019). Signal integration from these inputs determines phototactic responses (Bhaya 2004, Wilde and Mullineaux 2017, Harwood et al. 2021). Several of these signaling systems are homologous to the chemotaxis signal transduction systems (Wuichet and Zhulin 2010, Han et al. 2022) (Fig. S1). The canonical chemotaxis system of *Escherichia coli*, which controls flagellar motility, utilizes a transmembrane receptor called methyl-accepting chemotaxis protein (MCP), which is connected to the histidine kinase CheA through the adaptor protein CheW. Excitation of this signaling complex leads to autophosphorylation of a conserved histidine residue in the histidine phosphotransfer (Hpt) domain of CheA. The phosphoryl group is then transferred to an aspartate residue in the receiver domain (REC) of the response regulator CheY, which interacts with the flagellar motor to induce changes in the direction of flagellar rotation (Porter et al. 2011). Variations in this canonical chemotaxis system are used by many bacteria to control cellular

Received 15 February 2024; revised 14 May 2024; accepted 25 May 2024

© The Author(s) 2024. Published by Oxford University Press on behalf of FEMS. This is an Open Access article distributed under the terms of the Creative Commons Attribution Non-Commercial License (<https://creativecommons.org/licenses/by-nc/4.0/>), which permits non-commercial re-use, distribution, and reproduction in any medium, provided the original work is properly cited. For commercial re-use, please contact journals.permissions@oup.com

functions other than flagellar motility, such as twitching motility, exopolysaccharide production, and cellular aggregation (Bhaya et al. 2001, Whitchurch et al. 2004, He and Bauer 2014).

Wuichet and Zhulin (2010) classified cyanobacterial chemotaxis-like systems under the T4P-based motility group, which contains systems that typically have two CheY-like response regulators. Cyanobacterial systems frequently utilize photoreceptor modules, but lack proteins to modulate MCP methylation and adaptation. The absence of these methylation/demethylation enzymes is hypothesized to be a result of the directional light-sensing mechanism employed in cyanobacterial phototaxis, which eliminates the need to adapt to fluctuating signals over time (Wuichet and Zhulin 2010, Schuergers et al. 2016). In contrast to chemotaxis-like systems that control twitching motility in heterotrophic bacteria, the first CheY homolog in operons that encode cyanobacterial systems is a PatA-type response regulator comprising N-terminal PATAN and C-terminal REC domains (Makarova et al. 2006, Han et al. 2022). In *Synechocystis*, the response regulators PixE, LsiR, and Slr1594, which are not part of a chemosensory system, share this domain architecture. PixE forms a complex with the blue light sensor PixD, which dissociates upon illumination with blue light. Unbound PixE is able to elicit negative phototaxis (Ren et al. 2013, Sugimoto et al. 2017). LsiR triggers negative phototaxis in response to UV light, which induces *lsiR* expression (Song et al. 2011). It has been shown that in *Synechocystis*, the PATAN domain of these regulators localizes to the inner membrane and interacts with the N-terminal cytoplasmic domain of PilC and the pilus assembly ATPase PilB1. Importantly, overexpression of the truncated PixE containing only the PATAN domain is sufficient to switch phototactic orientation, suggesting that the PATAN domain is the principal output domain of at least those PatA-type regulators that control the direction of movement (Jakob et al. 2020, Han et al. 2022). The second CheY-like response regulator of cyanobacterial chemotaxis-like systems consists of a single REC domain. In *Synechocystis*, they localize mainly to the cytoplasm and do not interact with any components of the pilus motor (Kera et al. 2020, Han et al. 2022).

Synechocystis exhibits positive phototaxis toward wavelengths ranging from green to far-red, while negative phototaxis is elicited by blue or UV light (Choi et al. 1999, Ng et al. 2003, Savakis et al. 2012). Among the photoreceptors that control phototactic orientation, the cyanobacteriochrome PixJ (encoded by *sl0041* and *sl0042*) is essential for positive phototaxis (Yoshihara et al. 2000, Bhaya et al. 2001, Ng et al. 2003, 2004). This blue/green light sensor is a part of the chemotaxis-like system Tax1 (Fig. 1A), which comprises the CheA-like histidine kinase PixL (Sl0043), two CheW-like adaptor proteins (Sl0040 and Sl0044), CheY-like response regulator PixH (Sl0039), and PatA-type regulator PixG (Sl0038). Disruption of genes in the *tax1* operon, except for the *cheW* genes, resulted in mutants that showed negative phototaxis under light conditions, which triggered positive phototaxis in wild-type cells (Yoshihara et al. 2000, Bhaya et al. 2001, 2004). Moreover, mutating the phospho-accepting aspartate of PixG reverses the phototactic orientation (Han et al. 2022). Hence, it is likely that the Tax1 system establishes positive phototaxis by transducing light signals from the photoreceptor to its response regulators via a phosphorylation cascade. However, it is unclear whether PixG and PixH are phosphorylated and how these two regulators with disparate localization patterns cooperate to modulate phototaxis in *Synechocystis*.

To shed light on the *Synechocystis* Tax1 signal transduction pathway and understand the molecular mechanism by which this system determines movement direction, we evaluated the phospho-

transfer between the purified histidine kinase PixL and the regulators PixG and PixH *in vitro* and studied the motility phenotypes of phospho-acceptor site mutants *in vivo*. Our findings verified that both PixG and PixH are phosphorylated by PixL. Moreover, the phosphorylation of PixG enhances the interaction of PixG with the T4P motor at the light-facing site of the cell, whereas PixH acts as a phosphate sink that modulates PixG phosphorylation.

Materials and methods

Protein purification

The plasmids used for overexpression of 6xHis-tagged proteins are listed in Table S1. These plasmids were generated by amplifying *pixL^{AREC}* (residues 1–1253), *pixL_REC* (residues 1274–1402), *pixG*, and *pixH* via PCR with genomic DNA using primers (Table S2) to introduce BamHI and Sall restriction sites. The amplified products were cut and ligated into BamHI and Sall restriction sites of the pQE-80 L vector. The resulting plasmids were verified by sequencing. PixG and PixH variants were constructed using pQE-*pixG* and pQE-*pixH* via oligonucleotide-directed mutagenesis using the primers listed in Table S2.

Escherichia coli BL21(DE3) transformed with expression plasmids were grown in 500 ml LB medium supplemented with 100 µg/ml ampicillin. Protein expression was induced by adding 100 µM isopropyl-β-D-thiogalactopyranoside (IPTG) when the cells reached an OD₆₀₀ of 0.6, and the cultures were incubated at 18°C overnight. Cells were harvested by centrifugation at 4000 rpm, resuspended in lysis buffer (150 mM NaCl, 50 mM Tris/HCl, 20 mM imidazole, and pH 8.0) containing 250 µg/ml lysozyme and 20 µg/ml DNase, incubated on ice for 30 min, and then disrupted in a French press. The lysate was centrifuged at 16 500 g at 4°C for 30 min, and the supernatant was filtered through a 0.45-µm membrane to remove any remaining particulate material. The cleared lysate was loaded onto the column with 1 ml Ni-NTA resin at 4°C. The column was washed twice with 5 ml lysis buffer and eluted five times with 1 ml elution buffer (150 mM NaCl, 50 mM Tris-HCl, 500 mM imidazole, and pH 8.0). Eluted fractions were analyzed by SDS-PAGE, and the fractions with the highest yield were concentrated and further purified with a Superdex 200 10/300 GL column using reaction buffer (10 mM HEPES, 50 mM KCl, 0.1 mM EDTA, 1 mM DTT, 5 mM MgCl₂, 10% glycerol (v/v), and pH 8.0). The purified proteins were stored at –80°C.

Autophosphorylation and phosphotransfer assays

All phosphorylation experiments were performed in reaction buffer (see above). For autophosphorylation assays, 0.3 nmol purified PixL^{AREC} were incubated in 60 µl reaction buffer containing 0.5 mM ATP and 1 µCi [γ -³²P]ATP at 30°C. At the appropriate time, 7.8 µl aliquots were removed from the reaction and mixed with 4.2 µl loading buffer (4xNuPAGE™ LDS sample buffer (Invitrogen) supplemented with 100 mM DTT). The samples were separated on a 4%–12% Bis-Tris gel (NuPAGE™) using MES SDS running buffer (50 mM MES, 50 mM Tris Base, 0.1% SDS, 1 mM EDTA-Na₂, and pH 7.3), stained with Coomassie, and dried under vacuum. An autoradiograph was obtained using a Phosphor Imager (Typhoon FL 9500). For phosphotransfer assays between PixL^{AREC} and a single regulator, PixL^{AREC} was incubated with [γ -³²P]ATP for 4 min as described above. At the same time, a 7.8-µl aliquot was diluted with 7.8 µl reaction buffer and quenched by adding 8.4 µl loading buffer as the t₀ reference, and 35 µl of the reaction mixture was mixed with 35 µl reaction buffer containing an equimolar amount

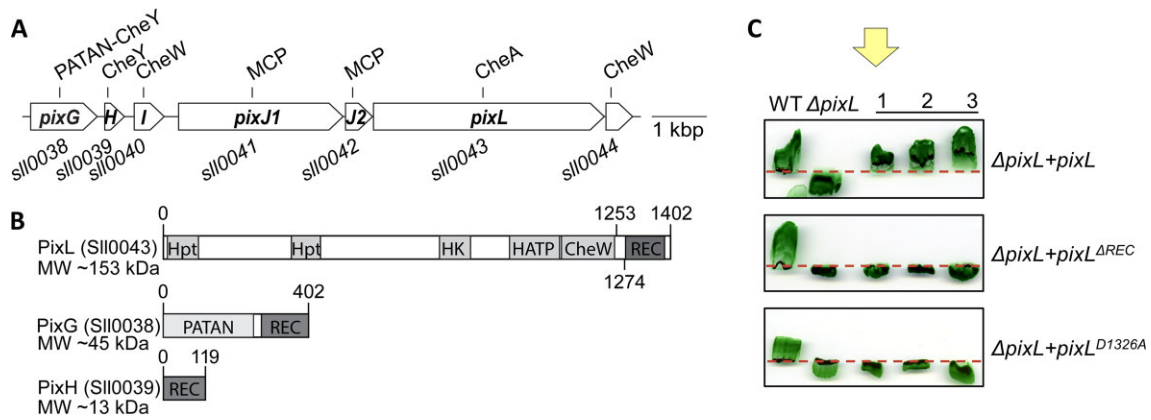


Figure 1. The REC domain of PixL is essential for positive phototaxis. (A) Schematic representation of gene organization of the Tax1 system in *Synechocystis*. Homology to chemotaxis systems is shown at the top, with gene names indicated within the arrows and locus names at the bottom. (B) Domain architecture of histidine kinase and its cognate response regulators according to the KEGG sequence similarity database. For PixL, the start and end positions of the truncated proteins used in this study are provided. (C) Phototaxis experiments of wild-type *Synechocystis*, a Δ pixL mutant, and strains expressing PixL, PixL^{AREC}, or PixL^{D1326A} in the Δ pixL background. Protein expression was induced using copper-free medium. Cells were spotted on 0.5% (w/v) BG-11 motility agar and exposed to directional white light ($\sim 50 \mu\text{mol photons m}^{-2} \text{ s}^{-1}$) for ~ 4 days. The arrow indicates the direction of illumination, and the dotted line indicates the initial positions of the cells.

of the purified regulator. The phosphotransfer reaction was incubated at 30°C, terminated at the indicated time points, and processed, as described above. For phosphotransfer assays with both regulators, PixL^{AREC} was initially phosphorylated for 4 min. Subsequently, 20 μl of this reaction and a 20- μl aliquot containing equimolar amounts of both regulators were mixed, resulting in a 2.5- μM concentration of each protein in the reactions, and processed in the same way as the other assays.

Culture conditions and strains

Synechocystis sp. PCC 6803 substrain PCC-M (Trautmann et al. 2012) and mutant strains (Table S1) were propagated on BG-11 agar plates (0.75% (w/v) supplemented with 0.3% (w/v) sodium thiosulfate) at 30°C under continuous white light illumination (Philips TLD Super 80/840) of 50 $\mu\text{mol photons m}^{-2} \text{ s}^{-1}$. For strains encoding expression cassettes under the control of the *petJ* promoter, CuSO₄ free BG-11 medium was used to induce protein expression, whereas 2.5 μM CuSO₄ was added to repress it. Mutant strains were supplemented with appropriate antibiotics at concentrations of chloramphenicol (7 $\mu\text{g/ml}$), streptomycin (10 $\mu\text{g/ml}$), kanamycin (50 $\mu\text{g/ml}$), and gentamycin (10 $\mu\text{g/ml}$).

Mutagenesis and plasmid construction

The plasmids and primers used are listed in Table S1 and S2, respectively. The Δ pixL strain was generated by transforming *Synechocystis* cells with the plasmid pUC- Δ pixL, which was constructed using PCR-based seamless assembly cloning (Beyer et al. 2015). For complementation, Δ pixL was transformed with plasmids constructed as follows: genes *pixL* and *pixL*^{AREC} were amplified from genomic DNA using primers to introduce EcoRI and BamHI restriction sites and subsequently cut and ligated into the appropriate restriction site of the pUR-expression vector harboring an N-terminal FLAG sequence (Wiegard et al. 2013). The pUR-*pixL*^{D1326A}-flag variant was generated using the Q5 Site-Directed Mutagenesis Kit (NEB). Response regulator variants harboring a mutant *pixG* or *pixH* gene were generated using the Q5 Site-Directed Mutagenesis Kit (NEB) and the primers listed in Table S2. The resulting plasmids were used to transform Δ pixLGH or wild-type cells. To create Δ pixD+*pixG*-*eyfp* and Δ pixD+*pixG*^{D326A}-*eyfp*, WT+*pixG*-*eyfp* and WT+*pixG*^{D326A}-*eyfp* mutants were transformed with the genomic

DNA of the Δ pixD strain. Complete segregation of these mutants was confirmed by colony PCR.

To create pGBK-*pixG*^{D326A} for the Y2H assay, the *pixG* gene was amplified from *Synechocystis* genomic DNA using the primers listed in Table S2 and cloned into the pJET1.2 vector (CloneJET PCR cloning kit, ThermoFisher). The resultant plasmid pJET1.2-*pixG* was further used to create pJET1.2-*pixG*^{D326A} by site-directed mutagenesis. The pJET1.2-*pixG*^{D326A} was digested with restriction endonucleases BamHI and SpeI and ligated into the corresponding restriction sites of pGBKT7. All other plasmids used for Y2H assays have been described previously (Jakob et al. 2020, Han et al. 2022).

Phototaxis assays

Cells from freshly grown plates were resuspended and spotted or directly restreaked onto 0.5% (w/v) BG-11 agar plates containing 0.3% (w/v) sodium thiosulfate, 0.2% glucose, and 10 mM TES buffer (pH 8.0). CuSO₄ was omitted from the medium to induce the *petJ* promoter or was added at a concentration of 2.5 μM to inhibit expression. After 2–3 days of incubation under diffuse low-intensity white light, the plates were transferred to nontransparent boxes with a one-sided opening (15 or 50 $\mu\text{mol photons m}^{-2} \text{ s}^{-1}$ at the front of the boxes) for 4–13 days. For a detailed protocol, see Jakob et al. (2017).

Single-cell tracking

Single-cell motility assays were performed as previously described (Jakob et al. 2017). Briefly, cells from the leading edge of a colony on the phototaxis assay plate were resuspended in fresh BG-11 medium. A 3- μl droplet of the suspension was spotted on 0.3% (w/v) BG-11 agarose plates and left to dry for 15 min. The *petJ* promoter was induced by omission of copper from the medium. The cells were carefully covered with a coverslip and a silicone ring to prevent evaporation and stabilize the surface. After a 2-h dark incubation and 3-min lateral illumination under white light (fluence rate $\sim 50 \mu\text{mol photons m}^{-2} \text{ s}^{-1}$, high luminous output golden white LED lamp (Yoldal) or RGB-LED (625/525/470 nm) (World Trading Net)), a 3–5 min time-lapse video was recorded at room temperature with one frame every 3 s using an upright Nikon Eclipse Ni-U microscope fitted with a 40x objective (numer-

ical aperture 0.75). Cell tracking was performed using ImageJ and the TrackMate plugin (Ershov et al. 2022). The tracks were further analyzed using a custom R script. Only cells tracked for at least 10 consecutive frames were analyzed. Additionally, cells displaying displacement of at least 0.5 μm and a speed of at least 0.02 $\mu\text{m s}^{-1}$ were classified as motile tracks.

Y2H analysis

The Y2H analysis was performed as previously described (Jakob et al. 2020). Briefly, yeast transformants containing bait-prey pairs were selected on a complete supplement mixture dropout medium lacking leucine and tryptophan at 30°C for 4 days. Subsequently, the cells were screened for interactions by streaking on dropout medium lacking leucine, tryptophan, and histidine supplemented with 5 mM 3-amino-1,2,4-triazole (3-AT) at 30°C for 6–7 days.

Confocal laser scanning microscopy

Cells from fresh phototaxis plates were resuspended and spotted onto 0.3% agarose BG-11 plates as described for single-cell motility assays. All plates and media were incubated at 30°C prior to experiments. After the droplets had dried at 30°C, the cells were excised with an agarose block from the plate and carefully flipped into a 35-mm glass bottom μ -Dish (ibidi GmbH) such that the cells were positioned between glass and agarose. Confocal microscopy imaging was performed at room temperature with a Nikon A1 confocal system on an inverted Nikon Eclipse Ti microscope using a 60x oil immersion (refractive index 1.515) objective with a numerical aperture of 1.4. Cells were exposed to directional red light emitted by an RGB-LED (peak 625 nm, World Trading Net) at a fluence rate of $\sim 75 \mu\text{mol photons m}^{-2} \text{s}^{-1}$. The LED was fixed to the microscope stage, and the emission angle was limited by wrapping the LED bulb with a tape. After an incubation period of ~ 10 min, the cell position in the scanned area and phototactic behavior were first assessed by imaging chlorophyll autofluorescence with the 640 nm laser line in a 3-min time-lapse series at one frame every 3 s. To visualize eYFP signal localization and allow resolution of differential signal distribution, a region of interest was then selected and magnified by an additional zoom factor of 4.3 (scan area of 49.42 $\mu\text{m} \times 49.42 \mu\text{m}$ at 512 pixels \times 512 pixels) and scanned with the 514-nm laser recording 3-min time-lapse series as before.

To determine fluorescence polarity and intensity at the cell periphery, time-lapse series were analyzed using a custom macro in ImageJ, which detects cells automatically and measures radial intensity via the Radial Profile Extended plugin (Carl 2006). Here, the intensity was integrated as a function of the radius in 10° sectors around the detected cells in each slice of the time-lapse stack. Cell tracking information was obtained as previously described for single-cell motility assays using the TrackMate plugin (Ershov et al. 2022). Radial intensity and tracking data were then further analyzed and correlated at the single-cell level with a custom R script using the circular package (Agostinelli and Lund 2022). Conceptually, to identify the maximum fluorescence angle per cell, we measured integrated intensities of 90° sectors, which were rotated in 10° steps around the cell. Of the resulting 36 sectors, the mean angle of the 90° sector with the highest total intensity was defined as the maximum intensity angle. Radial fluorescence intensity measurements were assigned to tracked cells using the nearest neighbor search function from the RANN package (Arya et al. 2019). Finally, the mean of the maximum intensity angle over the first five time points was calculated to avoid introducing

additional noise due to photobleaching over the full 3-min video. The entire length of the video was used to calculate the displacement angle as the angle of displacement between the first and last frames of the track. Scripts used for the acquisition of radial intensity measurements in ImageJ, as well as data processing and analysis in R (R Core Team 2023), are available in the GitHub repository https://github.com/jonas-hammerl/Tax1_Synechocystis.

Results

The REC domain of PixL is involved in phototaxis regulation

The putative histidine kinase PixL of *Synechocystis* comprises two N-terminal Hpt domains, a catalytic core, and a C-terminal REC domain, which is absent in the histidine kinase of the *E. coli* Che system (Fig. 1B). To elucidate the role of the REC domain of PixL in phototaxis control, we complemented a ΔpixL mutant in *Synechocystis* with plasmids for the expression of FLAG-tagged PixL ($\Delta\text{pixL}+\text{pixL}$) or truncated PixL without the REC domain ($\Delta\text{pixL}+\text{pixL}^{\text{AREC}}$; PixL^{AREC} residues 1–1253). Consistent with previous studies (Yoshihara et al. 2000, Bhaya et al. 2001), ΔpixL exhibited negative phototaxis under white-light illumination, which induced positive phototaxis in the wild type (Fig. 1C). Subsequently, we investigated the phototaxis of the complementation strains. Expression of the FLAG-tagged PixL variants from the *petJ* promoter, which is induced under copper limitation, was confirmed by western blot analysis (Fig. S2). Under inducing conditions, only wild-type PixL restored the positive phototaxis in the ΔpixL mutant strain (Fig. 1C). To determine whether the phosphorylation of the REC domain is essential for its function, we attempted to complement the ΔpixL mutant with a plasmid expressing the phosphorylation-deficient PixL^{D1326A} variant ($\Delta\text{pixL}+\text{pixL}^{\text{D1326A}}$). Although western blot analysis established that PixL^{D1326A} was expressed at levels comparable to those of full-length and truncated proteins (Fig. S2), the mutant protein was unable to restore positive phototaxis (Fig. 1C), indicating that an intact phosphorylation site in the REC domain was required for positive phototaxis. This implies that an additional phosphorylation step in the PixL REC domain modulates the PixL kinase activity.

PixL phosphorylates both PixG and PixH

Next, we wanted to confirm phosphotransfer between PixL and its cognate CheY-like response regulators PixG and PixH *in vitro*. Therefore, we purified the recombinant proteins bearing a 6 \times His affinity tag at the N-terminus, which were expressed in *E. coli* BL21(DE3), and incubated them with [γ -³²P]ATP. However, we did not detect stable autophosphorylation of purified full-length PixL or substantial phosphoryl transfer to its cognate response regulators (Fig. S3). Considering that the PixL REC domain might participate in intermolecular phosphotransfer and earlier reports that the REC domain of chemosensory histidine kinases from other bacteria interferes with the autophosphorylation of their kinase domain (Inclán et al. 2008, Silversmith et al. 2016), we analyzed the truncated variant of the histidine kinase PixL^{AREC}. Recombinant PixL^{AREC} was shown to be capable of stable autophosphorylation *in vitro* upon incubation with [γ -³²P]ATP (Fig. 2A). Further, we studied whether PixL^{AREC} can phosphorylate the PixL receiver domain. Therefore, a separate PixL_REC domain (residues 1274–1402) was expressed in *E. coli* and incubated with phosphorylated PixL^{AREC} (Fig. S4). PixL_REC can be phosphorylated by PixL^{AREC}. However, this phosphorylation event is transient, and phosphorylated PixL_REC can only be detected for around 1 min. Together

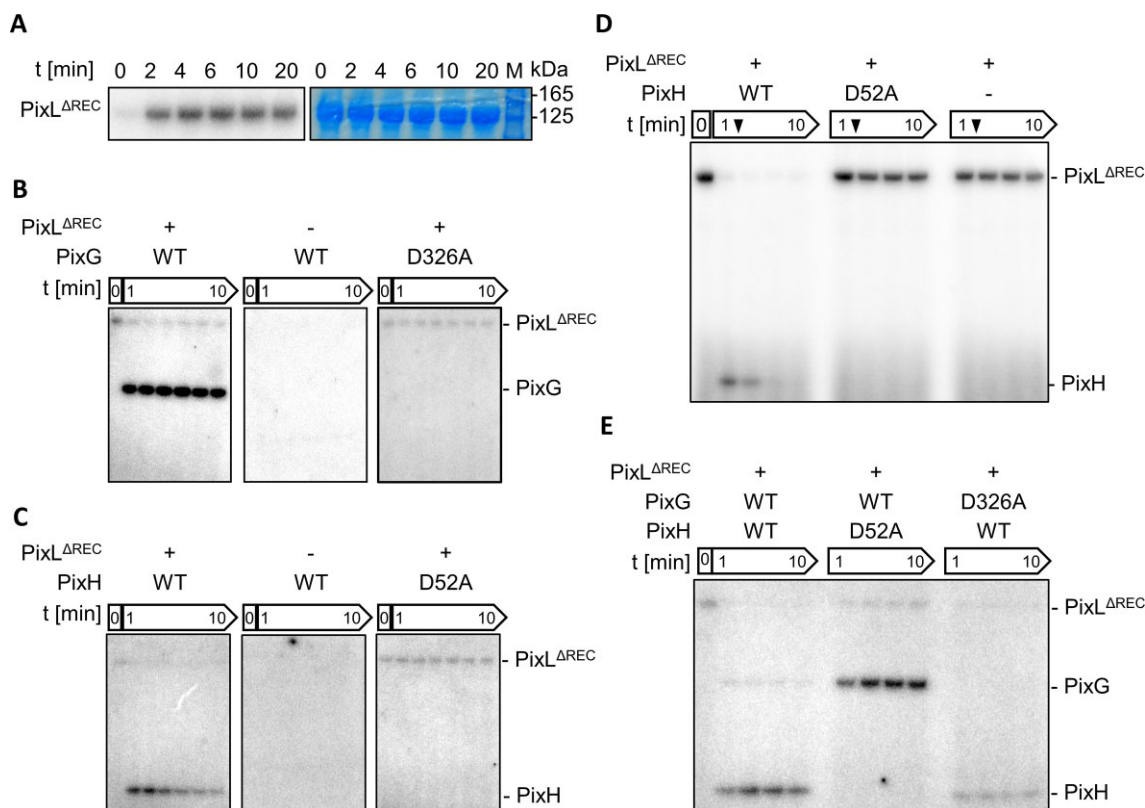


Figure 2. Autophosphorylated PixL transfers phosphate to the response regulators PixG and PixH, and PixH modulates PixG phosphorylation. (A) Autoradiograph (left) and Coomassie stain (right) of PixL^{ΔREC}. 0.3 nmol protein was incubated in 60 μl reaction buffer containing 1 μCi [γ -³²P]ATP and 500 μM ATP at 30°C. Aliquots were quenched in loading buffer at the indicated time points. The samples were separated on a 4%–12% Bis-Tris SDS-PAGE gel, stained with Coomassie, dried under vacuum, and visualized by autographic exposure. Lane M, molecular weight marker (kDa). His-PixL^{ΔREC}, 138 kDa. (B, C) Autoradiographs of phosphotransfer assays with PixL^{ΔREC} and PixG or PixH, and the respective phosphorylation-deficient mutants. As described above, 0.3 nmol PixL^{ΔREC} was incubated with [γ -³²P]ATP for 4 min. At t₀, the PixL^{ΔREC} phosphorylation reaction was mixed 1:1 with equimolar amounts of wild-type or mutant PixG or PixH in reaction buffer. The phosphotransfer reactions were incubated at 30°C and aliquots were sampled at 1, 2, 4, 6, 8, and 10 min. As a negative control, PixL^{ΔREC} was omitted from the reactions. (D) Phosphotransfer assays containing 2.5 μM of PixL^{ΔREC} and 5 μM PixH. PixL^{ΔREC} was incubated with [γ -³²P]ATP for 4 min prior to the addition of the PixG or PixH variants at t₀. The phosphotransfer reaction was incubated at 30°C and aliquots were sampled at 1 min, after which 100x excess of unlabeled ATP was added at 2 min (arrowhead), and after 3, 7, and 10 min. The samples were processed as before. (E) Autoradiograph of tripartite phosphotransfer assays containing 2.5 μM of PixL^{ΔREC}, PixG, and PixH in the combinations listed. PixL^{ΔREC} was autophosphorylated for 4 min and aliquots of the transfer reaction were sampled at 1, 3, 7, and 10 min and processed as before.

with the observation that full-length PixL is inactive, this suggests that the REC domain is a negative regulator of PixL kinase activity and facilitates the rapid dephosphorylation of the protein.

To investigate phosphotransfer from histidine kinase PixL to its cognate response regulators, purified recombinant PixG and PixH were incubated with [γ -³²P]ATP alone or in the presence of PixL^{ΔREC}. Autoradiography revealed that both PixG and PixH were phosphorylated in the presence of PixL^{ΔREC} (Fig. 2B and C). Quantification of the radioactive signals indicated that in contrast to stable PixG phosphorylation, the phosphorylation level of PixH decreased over time (Fig. S5), suggesting that PixH had a higher rate of dephosphorylation.

The potential phosphorylation sites of the PixG and PixH receiver domains are aspartate 326 and aspartate 52, respectively (Han et al. 2022). To validate the specific phosphorylation sites, we repeated the phosphotransfer assays with response regulator variants in which the conserved aspartates were replaced by alanine. Purified PixG^{D326A} and PixH^{D52A} were not phosphorylated in the presence of PixL^{ΔREC} and radioactively labeled ATP, indicating that D326 and D52 are the only sites that accept a phosphoryl group from PixL (Fig. 2B and C). Equal loading and protein stability

were validated via Coomassie staining after SDS-PAGE separation (Fig. S6A and B)

To understand the low level of PixH phosphorylation, we aimed to differentiate between the slow phosphorylation of PixH by PixL^{ΔREC} and the rapid (auto-)dephosphorylation of the response regulator. To achieve this, we traced the radioactively labeled phosphoryl groups in a phosphotransfer assay spiked with a 100 times excess of unlabeled ATP after 2 min (Fig. 2D). These results clearly show that PixL^{ΔREC} autophosphorylation remained stable over the observed 10 min in the absence of PixH. However, when PixH was present, the histidine kinase promptly transferred all labeled phosphoryl groups to PixH, which was consequently dephosphorylated in less than 4 min. Previous studies have indicated that additional CheY regulators in a chemosensory pathway can facilitate the dephosphorylation of the main regulator (Sourjik and Schmitt 1998) or indirectly counteract its phosphorylation (Kühn et al. 2023). Considering the marked dephosphorylation of PixH, we hypothesized that this regulator might modulate PixG phosphorylation. To test this, we performed a phosphotransfer assay including the histidine kinase PixL^{ΔREC} and both regulators PixH and PixG. Compared to the phosphorylation assays with single response regulators (Fig. 2B and C), PixH displayed

enhanced phosphorylation in the presence of PixG, which, in turn, was phosphorylated to a much lower extent (Fig. 2E). In contrast, the addition of the nonphosphorylatable cognate response regulator to the assay had no detectable effect on the phosphorylation of PixH or PixG (Fig. 2E). The presence of proteins was verified using Coomassie-stained gels (Fig. S6C and D).

Phosphorylation is essential for the function of the response regulators PixG and PixH

To investigate the role of phosphorylation in the regulation of phototaxis by PixG and PixH, we analyzed the phototactic movement of *Synechocystis* strains expressing phosphorylation-deficient PixH^{D52A} or PixG^{D326A} variants from the native *tax1* locus (Fig. 3A). As previously demonstrated, only the Δ *pixGH*+*pixGH* strain, which expresses wild-type *pixG* and *pixH* in a Δ *pixGH* mutant but not the strain expressing a *pixG*^{D326A} variant, restored positive phototaxis (Han et al. 2022). In addition, we show that the Δ *pixGH*+*pixGH*^{D52A} mutant also displays negative phototaxis, as opposed to the positive phototactic behavior of the Δ *pixGH*+*pixGH* complementation strain (Fig. 3A), which is consistent with the previously shown negative phototaxis phenotype of the *pixH* mutant (Yoshihara et al. 2000). Moreover, we assessed the phototactic responses of the different strains at the single-cell level. We used lateral white LED irradiation to illuminate *Synechocystis* mutant strains freshly spotted on 0.3% (w/v) BG-11 agarose plates and recorded 5-min time-lapse videos using an upright Nikon Eclipse Ni-U microscope fitted with a 40x objective lens. Tracks of individual cells were measured, and the correlation between the direction of movement and the position of the white light source was calculated using a Rayleigh test (Fig. 3B). In accordance with the findings from the macroscopic phototaxis assay, the wild-type ($r = 0.588$) and Δ *pixGH*+*pixGH* ($r = 0.896$) cells moved toward light, whereas Δ *pixGH* ($r = -0.361$), Δ *pixGH*+*pixG*^{D326A}*H* ($r = -0.438$), and Δ *pixGH*+*pixGH*^{D52A} ($r = -0.310$) strains exhibited negative phototaxis. These results indicate that phosphorylation of both PixG and PixH is essential for positive phototaxis of *Synechocystis*. The single-cell tracking data (Table S3) reveals no apparent difference in cell speed between the wild type and the mutants exhibiting negative phototaxis that could account for the slower spread observed in macroscopic colonies. Rather, this can be attributed to a diminished orientation along the light vector as indicated by smaller absolute r values. This observation aligns with the hypothesis that the photoreceptor PixJ enhances the directionality of movement by increasing the polarization of pilus activity (Chau et al. 2015).

PixG was previously reported to interact directly with the extension motor PilB1 and the T4P platform protein PilC (Han et al. 2022). A yeast two-hybrid approach was used to investigate whether mutating the phosphor-accepting aspartate of PixG modulates this interaction. Yeast cells were transformed with prey vectors expressing PilB1 or the N-terminal cytoplasmic domain of PilC and bait vectors expressing either wild-type PixG or phosphorylation-deficient PixG^{D326A}. The selective growth of the transformants corroborates that PixG can interact with PilB1 and the N-terminus of PilC. However, these interactions significantly diminished in the presence of PixG^{D326A} (Fig. 3C, Fig. S7). Heterologously expressed PixG is unlikely to be phosphorylated in yeast. Drawing parallels from *E. coli* CheY, which shows a low level of activity in its unphosphorylated state (Barak and Eisenbach 1992), we argue that PixG exhibits low affinity for its binding partner, PilB1 and that the D326A mutation decreases this basal affinity, probably by hindering switching to a conformation that is inter-

mediate between inactive and active states (Dyer and Dahlquist 2006). Taken together, the phenotypic loss of function of PixG^{D326A} and its lack of interaction with T4P motor components suggest that only phosphorylated PixG binds to the T4P motor to promote positive phototaxis.

Phosphorylated PixG localizes to the leading cell pole and promotes positive phototaxis

In a previous study, we observed that PixG was localized at the cell membrane, whereas PixH was evenly distributed in the cytoplasm (Han et al. 2022). We speculated that phosphorylation-deficient PixG and PixH might exhibit altered cellular localization. Therefore, we created fluorescently tagged mutant variants and observed their cellular localization. Previous studies on PixE indicate that C-terminal tagging with GFP variants does not impair the function of PatA-like regulators to switch the phototactic orientation of *Synechocystis* (Jakob et al. 2020). To avoid any polar effects on the expression of the *tax1* operon and to clearly show the fluorescence signal, an expression cassette consisting of a copper-repressed *petJ* promoter controlling the expression of either *pixG* or *pixH* variants fused to eYFP at the C-terminus was inserted into a neutral locus on the chromosome of the wild-type *Synechocystis* strain. Epifluorescence imaging revealed that the phosphorylation-deficient proteins did not change their localization patterns considerably. PixG^{D326A} localizes to the cytoplasmic membrane, and PixH^{D52A} was still distributed in the cytoplasm with a small fraction near the membrane (Fig. S8).

The phenotypes of strains expressing fluorescently labeled PixG or PixG^{D326A} were also assessed using phototaxis assays and single-cell tracking (Fig. 4A and B). Both mutants showed the same positive phototactic response as the wild type under lateral white-light illumination regardless of the expression status. To evaluate the effect of enhanced PixG levels during negative phototaxis, we transformed a Δ *pixD* mutant with the *pixG* expression cassette. A Δ *pixD* photoreceptor mutant shows constitutive negative phototaxis under white or red illumination, because PixE is no longer bound to PixD (Masuda et al. 2004, Okajima et al. 2005). Overexpression of *pixG*^{D326A} in Δ *pixD* background cells led to negative phototaxis away from the white light source. In contrast, induction of the wild-type PixG fusion protein restored positive phototaxis in the Δ *pixD* background (Fig. 4C). This phototactic response was confirmed at the single-cell level; Δ *pixD*+*pixG*^{D326A}-*eyfp* ($r = -0.110$) behaved similarly to Δ *pixD* cells ($r = -0.087$), whereas the Δ *pixD*+*pixG*-*eyfp* strain ($r = 0.317$) exhibited positive phototaxis (Fig. 4D). These findings corroborate that only phosphorylated PixG can promote positive phototaxis, and suggest that elevated levels of phosphorylated PixG can counteract the effect of the phosphorylation-independent PatA-type regulator PixE (Han et al. 2022).

Based on these results, we hypothesized that in order to transduce light perception into polar T4P activity, phosphorylated PixG might localize differentially around the cell body. Therefore, we analyzed the distribution of membrane-bound PixG during cell movement. WT+*pixG*-*eyfp* and WT+*pixG*^{D326A}-*eyfp* cells resuspended from fresh, copper-free motility plates were spotted onto 0.3% (w/v) BG-11 agarose and eYFP fluorescence was imaged by confocal laser scanning microscopy either in the dark or under lateral, phototaxis-inducing red-light illumination. Single-cell tracking and radially resolved fluorescence intensity measurements from the time-lapse series revealed that without an external directional light stimulus, the displacement direction was unbiased. Both PixG-eYFP and PixG^{D326A}-eYFP signals were evenly

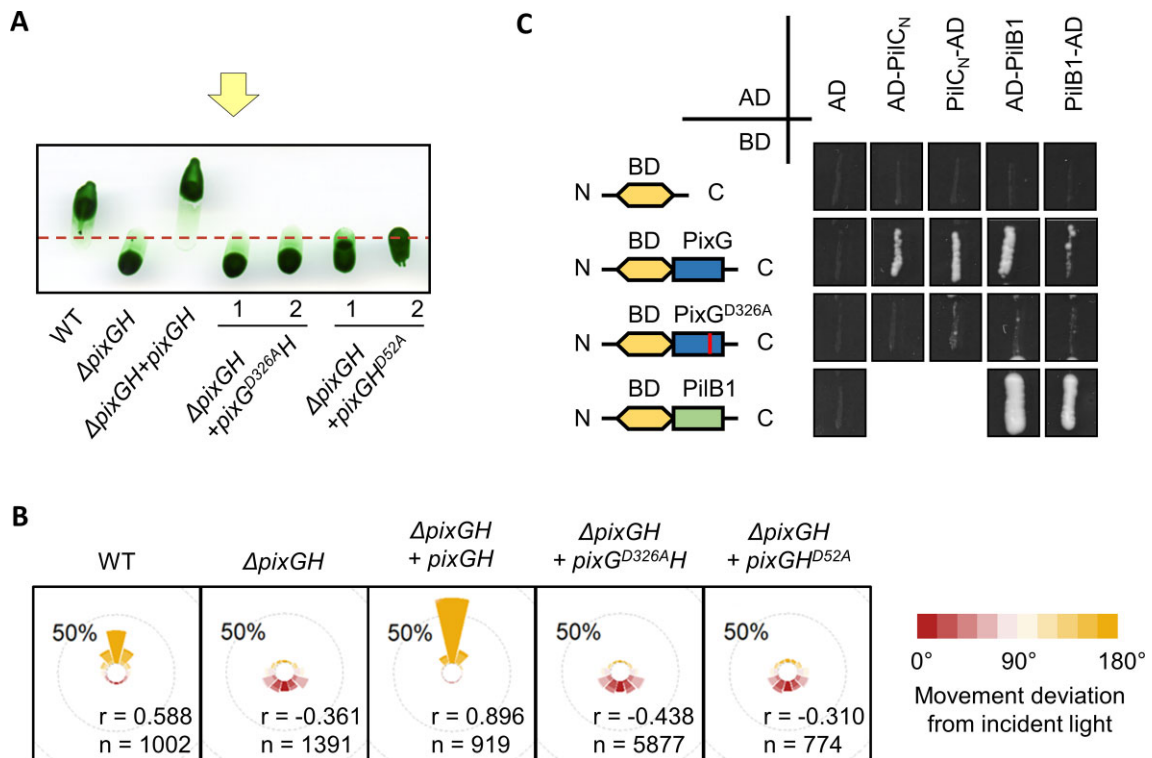


Figure 3. The phosphorylation of PixG and PixH is essential for positive phototaxis. (A) Phototaxis experiments of wild-type *Synechocystis*, a Δ pixGH mutant, and strains with both wild-type *pixG* and *pixH* (Δ pixGH+*pixGH*) or phosphorylation-deficient variants (Δ pixGH+*pixG*^{D326A}H and Δ pixGH+*pixG*^{D52A}H) reintroduced at the native locus. Cells were spotted onto 0.5% (w/v) BG-11 motility agar plates and placed under directional white light ($\sim 50 \mu\text{mol photons m}^{-2} \text{s}^{-1}$) for 5 days. The arrow indicates the direction of illumination, and the dotted line indicates the initial positions of the cells. (B) Histogram of the angular distribution of single-cell displacement during phototactic movement. Wild-type and mutant *Synechocystis* cells from motility plates were spotted onto 0.3% (w/v) BG-11 agarose and illuminated with a lateral white light LED (fluence rate of $\sim 50 \mu\text{mol photons m}^{-2} \text{s}^{-1}$). Cells from 5-min time-lapse videos were tracked. n = number of cells; r = mean resultant length from a Rayleigh test. (C) Yeast two-hybrid (Y2H) interaction assay of wild-type or phosphorylation-deficient PixG and PilB1, or the N-terminal cytoplasmic domain of PilC (PilC_N). For auxotrophic selection, cells harboring prey and bait vectors were grown on restrictive growth medium lacking tryptophan (–Trp) and leucine (–Leu) (Fig. S7). Plates lacking histidine (–His) and supplemented with 5 mM 3-AT were used to test for specific interactions. Empty prey and bait vectors were included as negative controls and PilB1 self-interaction was used as a positive control.

distributed along the cytoplasmic membrane. Under lateral red-light illumination, both WT+*pixG-eyfp* and WT+*pixG*^{D326A}-*eyfp* strains exhibited positive phototaxis toward the light, consistent with previous results (Fig. 4A and B). While *PixG*^{D326A}-eYFP remained evenly distributed as without directional light (Watson's U^2 test, $P > .10$), *PixG*-eYFP showed significant polarization towards the light-facing side of the cell compared to the dark control (Watson's U^2 test $P < .001$). The distribution of the directions of maximum *PixG*-eYFP fluorescence was highly correlated with the distribution of the displacement angles obtained from single-cell tracking [coefficient of overlapping $\Delta_4 = 0.808$ (where 1 means both functions are identical; Ridout and Linkie 2009), $P < .0001$], similar to the previously reported localization of PilB1-GFP toward the leading edge of motile cells (Schuergers et al. 2015). In summary, these findings support the idea that phosphorylated *PixG* activates PilB1 at the light-facing side of the cell to promote T4P formation, thereby inducing positive phototaxis. However, it remains unclear whether *PixG* actively recruits PilB1 to the T4P platform protein PilC or if it binds to PilB1, which has already been polarized through another mechanism.

Phosphorylatable PixH can counteract PixG function and impede positive phototaxis

The phenotype of the strains expressing fluorescently labeled PixH was examined at both the macroscopic and microscopic

scales (Fig. 5). Even though the overall phototactic response was severely limited, the mutant strains showed the same movement direction under lateral white light as the wild type when *PixH* expression was repressed (Fig. 5A). However, overexpression of the wild-type *PixH* fusion protein, but not the phosphorylation-deficient *PixH*^{D52A} variant, switched the phototactic orientation of the cells and resulted in negative phototaxis at the macroscopic scale (Fig. 5A). This switching was more readily observable at the single-cell level, with WT+*pixH-eyfp* exhibiting a pronounced negative phototactic movement ($r = -0.310$), whereas WT+*pixH*^{D52A}-*eyfp* showed clear positive phototaxis ($r = 0.394$) (Fig. 5B). Together with the findings from the phosphotransfer assays (Fig. 2D and E), these phototaxis experiments suggest that the enhanced expression of phosphorylatable *PixH* may switch phototactic orientation by influencing *PixG* phosphorylation. These results further imply that the *PixG* to *PixH* ratio in the cell is essential for phototaxis regulation.

Discussion

In *Synechocystis*, the chemotaxis-like Tax1 system is crucial for positive phototaxis (Yoshihara et al. 2000, Bhaya et al. 2001). However, how the signals perceived by the system's MCP-like green/blue photoreceptor *PixJ* modulate polar pilus activity is not understood. In this study, we demonstrated that the histidine ki-

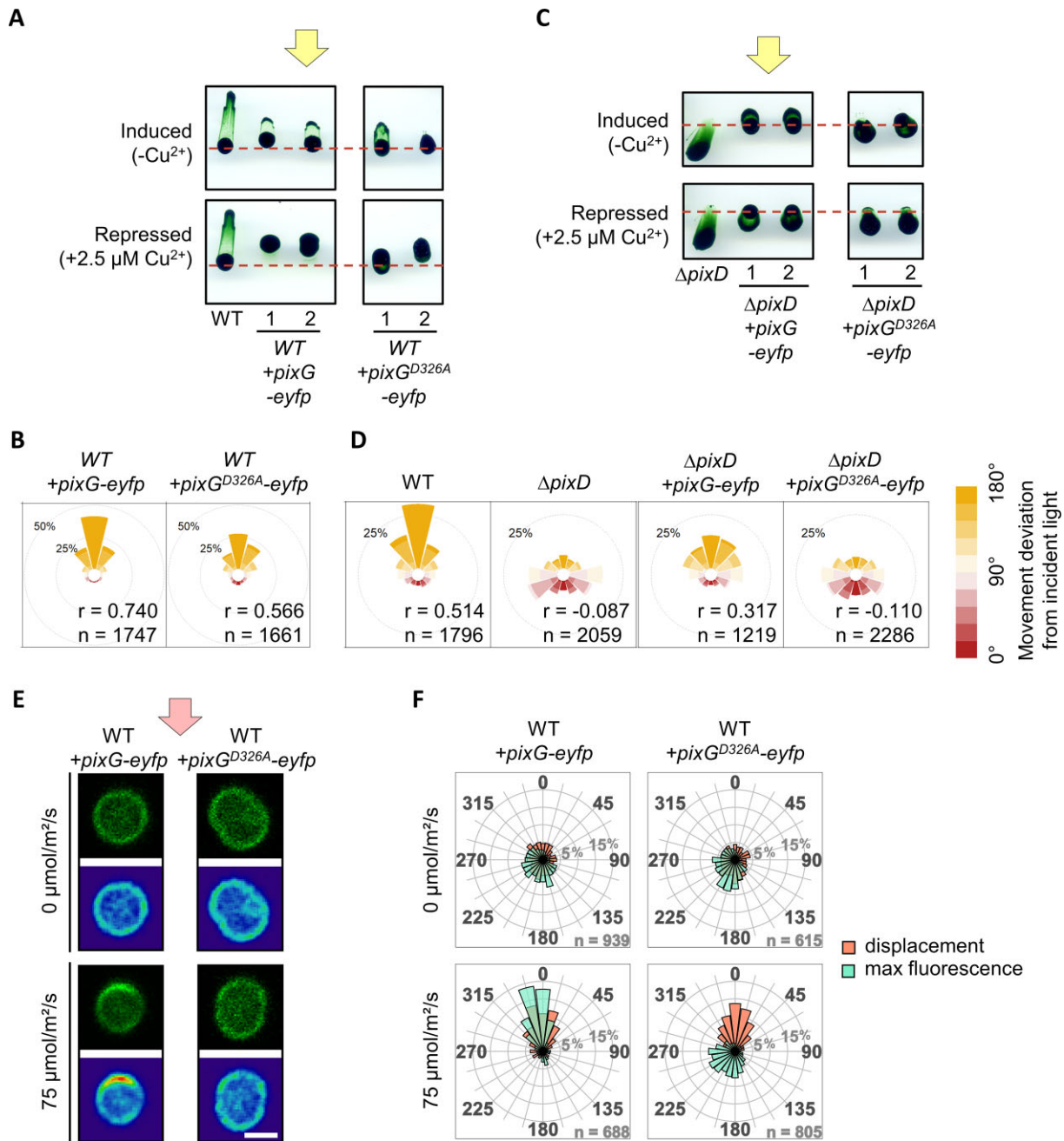


Figure 4. Phosphorylated PixG stimulates positive phototaxis and localizes to the leading pole of the cell (A) Phototaxis experiments of strains expressing either PixG or PixG^{D326A} as eYFP fusion proteins in a wild-type background (WT+pixG-eyfp and WT+pixG^{D326A}-eyfp). Cells were spotted on 0.5% (w/v) BG-11 motility agar and placed under directional white light ($\sim 15 \mu\text{mol photons m}^{-2} \text{ s}^{-1}$) for 7 days. Protein expression was induced in copper-free medium or inhibited by adding 2.5 μM CuSO₄. The arrow indicates the direction of illumination, and the dotted line indicates the starting positions of the cells. (B) Histogram of the angular distribution of single-cell displacement during phototactic movement of WT+pixG-eyfp and WT+pixG^{D326A}-eyfp. Cells from motility plates were spotted onto 0.3% (w/v) copper-depleted BG-11 agarose and illuminated with white light (fluence rate of $\sim 50 \mu\text{mol photons m}^{-2} \text{ s}^{-1}$). Cells from 5-min time-lapse videos were tracked. n = number of cells; r = mean resultant length from a Rayleigh test. (C) Phototaxis of strains expressing PixG or PixG^{D326A} in a ΔpixD background (ΔpixD+pixG-eyfp and ΔpixD+pixG^{D326A}-eyfp). The cells were incubated under directional white light ($\sim 50 \mu\text{mol photons m}^{-2} \text{ s}^{-1}$) for 10 days. (D) Histogram of the angular distribution of single-cell displacement during phototactic movement. Wild-type and mutant *Synechocystis* cells were illuminated with a lateral RGB-LED at an intensity of $\sim 50 \mu\text{mol photons m}^{-2} \text{ s}^{-1}$. Cells from 3-min time-lapse videos were tracked. (E) Representative confocal images of WT+pixG-eyfp and WT+pixG^{D326A}-eyfp cells on 0.3% agarose BG-11. eYFP was excited at 514 nm with or without a preceding 10 min lateral red-light stimulus ($75 \mu\text{mol photons m}^{-2} \text{ s}^{-1}$). In addition, a smoothed false-color image is displayed. Scale bar = 2 μm. (F) Histogram of the angular distribution of displacement and maximum fluorescence of strains quantified from 3-min time-lapse series of experiments as shown in (E). The lateral light source was located at 0°. n = number of tracks analyzed.

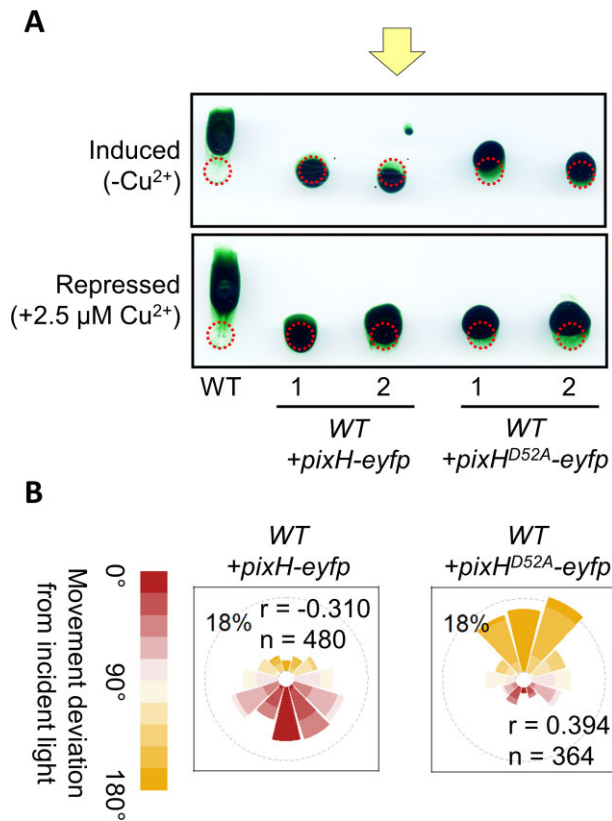


Figure 5. Overexpression of phosphorylatable PixH switches phototactic orientation. (A) *Synechocystis* cells expressing PixH (WT+*pixH-eyfp*) or PixH^{D52A} (WT+*pixH^{D52A}-eyfp*) were spotted on 0.5% (w/v) BG-11 motility agar and placed under directional white light ($\sim 50 \mu\text{mol photons m}^{-2} \text{ s}^{-1}$) for 13 days. Protein expression was induced in copper-free medium or inhibited by adding $2.5 \mu\text{M CuSO}_4$. The arrow indicates the direction of illumination, and the dotted circles indicate the starting positions of the cells. (B) Histogram of the angular distribution of single-cell displacement during phototactic movement of WT+*pixH-eyfp* and WT+*pixH^{D52A}-eyfp*. Cells from motility plates were spotted onto 0.3% (w/v) copper-depleted BG-11 agarose, illuminated with white light (fluence rate $\sim 50 \mu\text{mol photons m}^{-2} \text{ s}^{-1}$), and 5-min time-lapse videos were acquired. n = number of cells; r = mean resultant length from a Rayleigh test.

nase PixL phosphorylates both its cognate response regulators, PixH, and the PATAN-domain containing PixG, which have distinct roles in phototaxis regulation. Fundamentally, our experiments demonstrated that only phosphorylated PixG localized to the leading cell pole and promoted positive phototaxis, whereas PixH antagonized PixG function and prevented positive phototaxis. In *Synechocystis*, the PATAN domain of the nonphosphorylatable response regulator PixE alone is sufficient to bind to the pilus motor and change the orientation of phototaxis (Han et al. 2022). Likewise, the truncated PATAN domain of *Anabaena* PataA can complement a *patA* mutant (Young-Robbins et al. 2010). Consequently, we propose that PixG is the main output of the Tax1 system that mediates downstream signaling, and that phosphorylation of the PixG REC domain induces a conformational change that renders the PATAN domain accessible for protein interactions. Confocal laser scanning microscopy revealed that PixG, but not the phosphorylation-deficient PixG^{D326A}, was localized to the leading edge of moving cells under directional light. Hence, it is plausible that phosphorylated PixG stimulates positive phototaxis by interacting with the motility apparatus in a manner that leads to recruitment of PilB1 to the leading cell pole (Schuergers et al.

2015). This pattern mirrors the distribution of response regulators in chemotactic model organisms. For instance, in *Pseudomonas aeruginosa*, PilG phosphorylation by the histidine kinase ChpA enhances PilG localization to the leading cell pole, stimulating polarization of the extension motor PilB (Kühn et al. 2021, 2023). Similarly, in *M. xanthus*, FrzZ is recruited to the leading cell pole upon phosphorylation, and switches to the opposite pole during reversals (Kaimer and Zusman 2013).

Interestingly, overexpression of the PixG-eYFP fusion protein counteracted the induction of negative phototaxis by unbound PixE in a ΔpixD background (Fig. 4C and D). Elevated levels of non-phosphorylated PixG may compete with PixH for available phosphoryl groups or may prevent PixE from binding to pilus motor proteins. However, it is tempting to speculate that PixG could act as a positive regulator of PixL kinase activity, similar to the *M. xanthus* Frz system, in which the FrzZ response regulator positively regulates FrzE kinase activity (Kaimer and Zusman 2016). Regardless of the exact mechanism, we conclude that the regulation of PixG levels and the balance between different regulators are crucial for determining phototactic orientation. In this context, the distinct subcellular localization of the response regulators is noteworthy. Specifically, the recruitment of PixG to the leading cell pole should alter the local PixG-to-PixH ratio, potentially resulting in a self-amplifying signal.

Our phosphorylation assays revealed that the presence of phosphorylatable PixH reduced the amount of radiolabeled PixL^{AREC} and significantly diminished PixG phosphorylation (Fig. 2). Although these experiments demonstrated that PixH directly removes phosphates from PixL, this explanation does not account for the enhanced levels of phosphorylated PixH in the presence of PixG. Consequently, we cannot exclude the possibility of an (in-)direct phosphotransfer between the two response regulators.

These *in vitro* experiments may not fully replicate the complexity of the intracellular environment and do not directly confirm the phosphotransfer from PixL to PixG and PixH *in vivo*. Nonetheless, our observations align with the hypothesis that PixH acts as a phosphate sink in the Tax1 system *in vivo*. Such a mechanism, which allows rapid signal termination without the need for a phosphatase, has previously been described in chemotaxis systems with two response regulators that control flagellar responses (Sourjik and Schmitt 1998, Dogra et al. 2012). In the context of polarity control during twitching motility in *P. aeruginosa*, PilH has been suggested to act as a phosphate sink (Silversmith et al. 2016) although it was recently shown that it can modulate PilG phosphorylation independently of phosphotransfer to or from PilH (Kühn et al. 2023). Hence, our findings could also suggest that *Synechocystis* PixH functions either as a negative regulator, inhibiting PixL autophosphorylation, or as an enhancer of its dephosphorylation rate. Both models would allow PixH to terminate Tax1 signaling and explain the negative phototaxis phenotype of WT+*pixH-eyfp* (Fig. 5A). However, the requirement of phosphorylatable PixH for positive phototaxis, as indicated by the negative phototactic phenotype of $\Delta\text{pixGH}+\text{pixGH}^{\text{D52A}}$ (Fig. 3A and B), is not directly apparent. We speculate that adequate dephosphorylation of PixG is important for maintaining positive phototactic orientation.

The PixL REC domain is another intriguing player in the Tax1 signaling cascade. The REC domain of CheA homologs in other bacteria is known for its role in modulating kinase activity and its potential for phosphorylation via intramolecular phosphotransfer (Jiménez-Pearson et al. 2005, Risser et al. 2014, Silversmith et al. 2016, Kennedy et al. 2022). These studies have suggested that

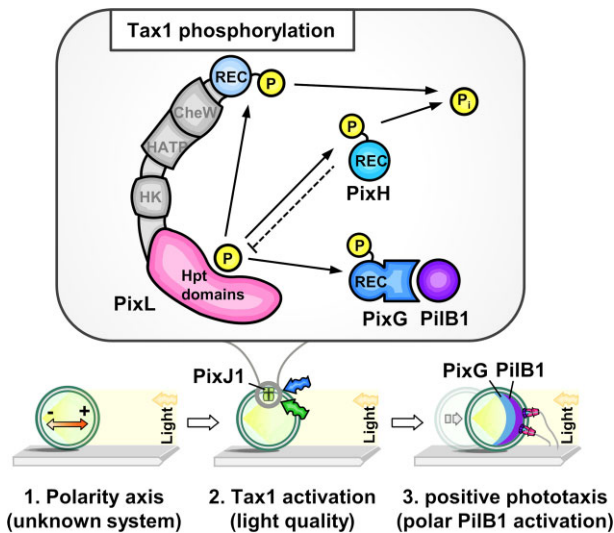


Figure 6. Regulation of positive phototaxis by the Tax1 system. Initially, the vector of incoming light sets up a polarity axis within the *Synechocystis* cells. The exact sensing mechanism is unknown, but it is assumed that light is sensed indirectly, potentially through changes in the proton motive force by the Tax3 system (Harwood et al. 2021). The kinase activity of PixL is modulated by the quality of light perceived by PixJ1. PixL undergoes autophosphorylation and transfers phosphoryl groups to its cognate response regulators PixG and PixH, as well as to its own REC domain, that facilitates rapid dephosphorylation. Phosphorylated PixG activates the extension motor PilB1 at the light-facing side of the cell, resulting in a switch from negative to positive phototaxis. PixH counteracts the function of PixG by reducing the phosphorylation of PixG. It probably serves directly as a phosphate sink, but it may also adjust PixL kinase activity. Inactivation of any of these Tax1 proteins solely inhibits positive phototaxis, underscoring that while the Tax1 system governs the reversal of cell orientation, it does not participate in the establishment of polarity itself.

the REC domain may act as a phosphate sink or may destabilize the phosphoryl group on the Hpt domain. Notably, the role of the REC domain as a phosphate sink has been proposed to be conserved, because genomes containing a single CheA with a REC domain generally lack chemosensory phosphatases (Berry et al. 2024). We found that only full-length PixL but not PixL^{D1326A} or PixL^{AREC} facilitate positive phototaxis. Moreover, only the truncated PixL^{AREC} but not the full-length kinase exhibited detectable autophosphorylation, which was rapidly diminished by the addition of its own REC domain *in vitro*. Based on these findings, we hypothesize that the PixL REC domain functions as a phosphate sink to eliminate phosphoryl groups from the Tax1 system for which no dedicated phosphatase has been identified. However, it may also shuttle phosphoryl groups to PixG or PixH or act through unidentified protein interaction partners.

While we have not yet delved into the activation of PixL by PixJ1 or the potential roles and affinities of the two Hpt domains of PixL, these areas present promising directions for future exploration. Our current work, however, has successfully provided a more nuanced model of positive phototaxis regulation by the Tax1 system in *Synechocystis* (Fig. 6), setting the stage for further investigations.

Synechocystis harbors two additional chemotaxis-like systems, each with two response regulators (Yoshihara et al. 2000, Bhaya et al. 2001, Han et al. 2022). For the Tax3 system, which is essential for pilus assembly, the PatA-type regulator PilG, but not the second response regulator PilH, strongly interacts with the cognate histidine kinase PilL and T4P motor components (Kera et al. 2020, Han et al. 2022). Furthermore, *pilH* mutants are hyperpili-

ated (Yoshihara et al. 2002). Albeit PilG is not strictly needed for pilus assembly (Bhaya et al. 2001), it seems plausible that Tax3 operates under the same regulatory principles as Tax1, with PilG targeting the pilus apparatus for assembly, and PilH antagonizing its function. Another motile single-celled cyanobacterium, *Synechococcus elongatus* UTEX 3055, has only one chemotaxis-like system for phototaxis (Yang et al. 2018). Interestingly, the inactivation of the *Synechococcus* Tax1 operon components led to random motility, and phototactic reversals were only observed in single GAF domain mutants of the multidomain photoreceptor PixJ, suggesting that the multiple GAF domains in this cyanobacteriochrome enable switching between positive and negative phototaxis. The role of the phosphorylation of response regulators of the Tax1 systems in *Synechococcus* has not yet been studied. However, in line with our proposed model, it was shown that enhanced induction of PixG expression supported positive phototaxis, whereas overexpression of PixH abolished phototactic motility (Yang et al. 2018).

Canonical chemotaxis systems in T4P-based motility typically harbor two response regulators, each with a single receiver domain (Wuichet and Zhulin 2010). In *P. aeruginosa*, the Chp system senses T4P attachment at one pole, leading to the phosphorylation of PilG by the histidine kinase ChpA. Phosphorylated PilG reinforces cell polarization by recruiting PilB to the sensing pole and locally activating T4P extension (Kühn et al. 2021, 2023). PilH becomes activated upon phosphorylation and disrupts the local positive feedback mechanism established by PilG, allowing cells to reverse. Our findings support the idea of a common regulatory mechanism for these sensory pathways. The primary regulator facilitates the polar activity of the pilus extension ATPase PilB, whereas the second regulator has an antagonistic function that is required to reverse cell polarity and switch movement orientation. While this leads to intermittent reversals necessary for chemotactic behavior in *P. aeruginosa*, it also leads to persistent positive phototaxis in *Synechocystis*.

Acknowledgments

We thank Sophia Engel and Werner Bigott for excellent technical support.

Supplementary data

Supplementary data is available at *FEMSML Journal* online.

Conflict of interest: None declared.

Funding

This work was funded by the Deutsche Forschungsgemeinschaft (DFG, German Research Foundation)—Project-ID 403222702-SFB 1381 to A.W. Y.H. was supported by the China Scholarship Council (CSC). J.H. was supported in part by the Ministry for Science, Research, and Arts of the State of Baden-Wuerttemberg We acknowledge support from the Open Access Publication Fund of the University of Freiburg.

References

- Agostinelli C, Lund U. R package ‘circular’: Circular Statistics (version 0.4-95). CRAN, 2022. <https://r-forge.r-project.org/projects/circular/> (1 March 2024, date last accessed).
- Arya S, Mount D, Kemp SE et al. RANN: Fast Nearest Neighbour Search (Wraps ANN Library) Using L2 Metric (version

- 2.6.1). CRAN, 2019. <https://CRAN.R-project.org/package=RANN> (1 March 2024, date last accessed).
- Barak R, Eisenbach M. Correlation between phosphorylation of the chemotaxis protein CheY and its activity at the flagellar motor. *Biochemistry* 1992;**31**:1821–26.
- Berry MA, Andrianova EP, Zhulin IB. Diverse domain architectures of CheA histidine kinase, a central component of bacterial and archaeal chemosensory systems. *Microbiol Spectr* 2024;**12**:e0346423. <https://doi.org/10.1128/SPECTRUM.03464-23>.
- Beyer HM, Gonschorek P, Samodelov SL et al. AQUA cloning: a versatile and simple enzyme-free cloning approach. *PLoS One* 2015;**10**:e0137652. <https://doi.org/10.1371/journal.pone.0137652>.
- Bhaya D. Light matters: phototaxis and signal transduction in unicellular cyanobacteria. *Mol Microbiol* 2004;**53**:745–54.
- Bhaya D, Bianco NR, Bryant D et al. Type IV pilus biogenesis and motility in the cyanobacterium *Synechocystis* sp. PCC6803. *Mol Microbiol* 2000;**37**:941–51.
- Bhaya D, Takahashi A, Grossman AR. Light regulation of type IV pilus-dependent motility by chemosensor-like elements in *Synechocystis* PCC6803. *Proc Natl Acad Sci USA* 2001;**98**:7540–5.
- Bischof LF, Friedrich C, Harms A et al. The Type IV pilus assembly ATPase PilB of *Myxococcus xanthus* interacts with the inner membrane platform protein PilC and the nucleotide-binding protein PilM. *J Biol Chem* 2016;**291**:6946–57.
- Carl P. Radial Profile Extended. 2006. <http://questpharma.u-strasbg.fr/html/radial-profile-ext.html> (1 March 2024, date last accessed).
- Chau RMW, Ursell T, Wang S et al. Maintenance of motility bias during cyanobacterial phototaxis. *Biophys J* 2015;**108**:1623–32.
- Choi J-S, Chung Y-H, Moon Y et al. Photomovement of the gliding cyanobacterium *Synechocystis* sp. PCC 6803. *Photochem Photobiol* 1999;**70**:95–102.
- Dogra G, Purschke FG, Wagner V et al. Sinorhizobium meliloti CheA complexed with ches exhibits enhanced binding to CheY1, resulting in accelerated CheY1 dephosphorylation. *J Bacteriol* 2012;**194**:1075–87.
- Dyer CM, Dahlquist FW. Switched or not?: the structure of unphosphorylated CheY bound to the N terminus of FliM. *J Bacteriol* 2006;**188**:7354–63.
- Ershov D, Phan MS, Pylvänäinen JW et al. TrackMate 7: integrating state-of-the-art segmentation algorithms into tracking pipelines. *Nat Methods* 2022;**19**:829–32.
- Han Y, Jakob A, Engel S et al. PATAN-domain regulators interact with the Type IV pilus motor to control phototactic orientation in the cyanobacterium *Synechocystis*. *Mol Microbiol* 2022;**117**:790–801.
- Harwood TV, Zuniga EG, Kweon H et al. The cyanobacterial taxis protein HmpF regulates type IV pilus activity in response to light. *Proc Natl Acad Sci USA* 2021;**118**:e2023988118. <https://doi.org/10.1073/pnas.2023988118>
- He K, Bauer CE. Chemosensory signaling systems that control bacterial survival. *Trends Microbiol* 2014;**22**:389–98.
- Inclán YF, Laurent S, Zusman DR. The receiver domain of FrzE, a CheA–CheY fusion protein, regulates the CheA histidine kinase activity and downstream signalling to the A- and S-motility systems of *Myxococcus xanthus*. *Mol Microbiol* 2008;**68**:1328–39.
- Jakob A, Nakamura H, Kobayashi A et al. The (PATAN)-CheY-like response regulator PixE interacts with the motor ATPase PilB1 to control negative phototaxis in the cyanobacterium *Synechocystis* sp. PCC 6803. *Plant Cell Physiol* 2020;**61**:296–307.
- Jakob A, Schuergers N, Wilde A. Phototaxis assays of *Synechocystis* sp. PCC 6803 at macroscopic and microscopic scales. *Bio Protoc* 2017;**7**:e2328. <https://doi.org/10.21769/BioProtoc.2328>
- Jakovljevic V, Leonardy S, Hoppert M et al. PilB and PilT are ATPases acting antagonistically in type IV pilus function in *Myxococcus xanthus*. *J Bacteriol* 2008;**190**:2411–21.
- Jiménez-Pearson MA, Delany I, Scarlato V et al. Phosphate flow in the chemotactic response system of *Helicobacter pylori*. *Microbiology* 2005;**151**:3299–311.
- Kaimer C, Zusman DR. Phosphorylation-dependent localization of the response regulator FrzZ signals cell reversals in *Myxococcus xanthus*. *Mol Microbiol* 2013;**88**:740–53.
- Kaimer C, Zusman DR. Regulation of cell reversal frequency in *Myxococcus xanthus* requires the balanced activity of CheY-like domains in FrzE and FrzZ. *Mol Microbiol* 2016;**100**:379–95.
- Kennedy EN, Barr SA, Liu X et al. *Azorhizobium caulinodans* chemotaxis is controlled by an unusual phosphorelay network. *J Bacteriol* 2022;**204**:e0052721. <https://doi.org/10.1128/JB.00527-21>
- Kera K, Yoshizawa Y, Shigehara T et al. Hik36-Hik43 and Rre6 act as a two-component regulatory system to control cell aggregation in *Synechocystis* sp. *Sci Rep* 2020;**10**:19405.
- Kühn MJ, Macmillan H, Talà L et al. Two antagonistic response regulators control *Pseudomonas aeruginosa* polarization during mechanotaxis. *EMBO J* 2023;**42**:e112165. <https://doi.org/10.15252/embj.2022112165>
- Kühn MJ, Talà L, Inclán YF et al. Mechanotaxis directs *Pseudomonas aeruginosa* twitching motility. *Proc Natl Acad Sci USA* 2021;**118**:e2101759118. <https://doi.org/10.1073/pnas.2101759118>
- Makarova KS, Koonin EV, Haselkorn R et al. Cyanobacterial response regulator PatA contains a conserved N-terminal domain (PATAN) with an alpha-helical insertion. *Bioinformatics* 2006;**22**:1297–301.
- Masuda S, Hasegawa K, Ishii A et al. Light-induced structural changes in a putative blue-light receptor with a novel FAD binding fold sensor of blue-light using FAD (BLUF); Slr1694 of *Synechocystis* sp. PCC6803. *Biochemistry* 2004;**43**:5304–13.
- Merz AJ, So M, Sheetz MP. Pilus retraction powers bacterial twitching motility. *Nature* 2000;**407**:98–102.
- Nakane D, Enomoto G, Bähre H et al. *Thermosynechococcus* switches the direction of phototaxis by a c-di-GMP-dependent process with high spatial resolution. *eLife* 2022;**11**:e73405. <https://doi.org/10.7554/eLife.73405>
- Nakane D, Nishizaka T. Asymmetric distribution of type IV pili triggered by directional light in unicellular cyanobacteria. *Proc Natl Acad Sci USA* 2017;**114**:6593–8.
- Ng WO, Grossman AR, Bhaya D. Multiple light inputs control phototaxis in *Synechocystis* sp. strain PCC6803. *J Bacteriol* 2003;**185**:1599–607.
- Okajima K, Yoshihara S, Fukushima Y et al. Biochemical and functional characterization of BLUF-type flavin-binding proteins of two species of cyanobacteria. *J Biochem* 2005;**137**:741–50.
- Porter SL, Wadhams GH, Armitage JP. Signal processing in complex chemotaxis pathways. *Nat Rev Micro* 2011;**9**:153–65.
- R Core Team. R: A Language and Environment for Statistical Computing. Vienna: R Foundation for Statistical Computing, 2023. <https://www.R-project.org/> (1 March 2024, date last accessed).
- Ren S, Sato R, Hasegawa K et al. A predicted structure for the PixD-PixE complex determined by homology modeling, docking simulations, and a mutagenesis study. *Biochemistry* 2013;**52**:1272–9.
- Ridout MS, Linkie M. Estimating overlap of daily activity patterns from camera trap data. *JABES* 2009;**14**:322–37.
- Risser DD, Chew WG, Meeks JC. Genetic characterization of the hmp locus, a chemotaxis-like gene cluster that regulates hormogonium development and motility in *Nostoc punctiforme*. *Mol Microbiol* 2014;**92**:222–33.

- Savakis P, De Causmaecker S, Angerer V et al. Light-induced alteration of c-di-GMP level controls motility of *Synechocystis* sp. PCC 6803. *Mol Microbiol* 2012;**85**:239–51.
- Schuergers N, Lenn T, Kampmann R et al. Cyanobacteria use micro-optics to sense light direction. *eLife* 2016;**5**:e12620. <https://doi.org/10.7554/eLife.12620>
- Schuergers N, Nürnberg DJ, Wallner T et al. PilB localization correlates with the direction of twitching motility in the cyanobacterium *Synechocystis* sp. PCC 6803. *Microbiology* 2015;**161**:960–6.
- Schuergers N, Wilde A. Appendages of the cyanobacterial cell. *Life* 2015;**5**:700–15.
- Silversmith RE, Wang B, Fulcher NB et al. Phosphoryl group flow within the *Pseudomonas aeruginosa* Pil-Chp chemosensory system: differential function of the eight phosphotransferase and three receiver domains. *J Biol Chem* 2016;**291**:17677–91.
- Song J-Y, Cho HS, Cho J-I et al. Near-UV cyanobacteriochrome signaling system elicits negative phototaxis in the cyanobacterium *Synechocystis* sp. PCC 6803. *Proc Natl Acad Sci USA* 2011;**108**:10780–5.
- Sourjik V, Schmitt R. Phosphotransfer between CheA, CheY1, and CheY2 in the chemotaxis signal transduction chain of *Rhizobium meliloti*. *Biochemistry* 1998;**37**:2327–35.
- Sugimoto Y, Nakamura H, Ren S et al. Genetics of the blue light-dependent signal cascade that controls phototaxis in the cyanobacterium *Synechocystis* sp. PCC6803. *Plant Cell Physiol* 2017;**58**:458–65.
- Takhar HK, Kemp K, Kim M et al. The platform protein is essential for type IV pilus biogenesis. *J Biol Chem* 2013;**288**:9721–8.
- Trautmann D, Voss B, Wilde A et al. Microevolution in cyanobacteria: re-sequencing a motile substrain of *Synechocystis* sp. PCC 6803. *DNA Res* 2012;**19**:435–48.
- Whitchurch CB, Leech AJ, Young MD et al. Characterization of a complex chemosensory signal transduction system which controls twitching motility in *Pseudomonas aeruginosa*. *Mol Microbiol* 2004;**52**:873–93.
- Wiegard A, Dörrich AK, Deinzer HT et al. Biochemical analysis of three putative KaiC clock proteins from *Synechocystis* sp. PCC 6803 suggests their functional divergence. *Microbiology* 2013;**159**:948–58.
- Wilde A, Mullineaux CW. Light-controlled motility in prokaryotes and the problem of directional light perception. *FEMS Microbiol Rev* 2017;**41**:900–22.
- Wiltbank LB, Kehoe DM. Diverse light responses of cyanobacteria mediated by phytochrome superfamily photoreceptors. *Nat Rev Micro* 2019;**17**:37–50.
- Wuichet K, Zhulin IB. Origins and diversification of a complex signal transduction system in prokaryotes. *Sci Signal* 2010;**3**:ra50. <https://doi.org/10.1126/scisignal.2000724>
- Yang Y, Lam V, Adomako M et al. Phototaxis in a wild isolate of the cyanobacterium *Synechococcus elongatus*. *Proc Natl Acad Sci USA* 2018;**115**:E12378–87.
- Yoshihara S, Geng X, Ikeuchi M. pilG gene cluster and split pilL genes involved in pilus biogenesis, motility and genetic transformation in the cyanobacterium *Synechocystis* sp. PCC 6803. *Plant Cell Physiol* 2002;**43**:513–21.
- Yoshihara S, Geng X, Okamoto S et al. Mutational analysis of genes involved in pilus structure, motility and transformation competency in the unicellular motile cyanobacterium *Synechocystis* sp. PCC 6803. *Plant Cell Physiol* 2001;**42**:63–73.
- Yoshihara S, Katayama M, Geng X et al. Cyanobacterial phytochrome-like PixJ1 holoprotein shows novel reversible photoconversion between blue- and green-absorbing forms. *Plant Cell Physiol* 2004;**45**:1729–37.
- Yoshihara S, Suzuki F, Fujita H et al. Novel putative photoreceptor and regulatory genes required for the positive phototactic movement of the unicellular motile cyanobacterium *Synechocystis* sp. PCC 6803. *Plant Cell Physiol* 2000;**41**:1299–304.
- Young-Robbins SS, Risser DD, Moran JR et al. Transcriptional regulation of the heterocyst patterning gene *patA* from *Anabaena* sp. strain PCC 7120. *J Bacteriol* 2010;**192**:4732–40.